

Electronic Supplementary Information (ESI)

**A glucose-activatable trimodal glucometer self-
assembled from glucose oxidase and MnO₂
nanosheets for diabetes monitoring**

**Jin-Long Chen,^{*abc†} Li Li,^{ac†} Shuo Wang,^{ac} Xiao-Yan Sun,^d
Lu Xiao,^{ac} Jia-Shu Ren,^{ac} Bin Di,^{ac} and Ning Gu^{*b}**

^aDepartment of Pharmaceutical Analysis, School of Pharmacy, China Pharmaceutical University,
Nanjing 210009, P. R. China

^bJiangsu Key Laboratory for Biomaterials and Devices, School of Biological Science and Medical
Engineering, Southeast University, Nanjing, 210096, P. R. Chin

^cKey Laboratory of Drug Quality Control and Pharmacovigilance (China Pharmaceutical
University), Ministry of Education, Nanjing 210009, P. R. China

^dLaboratory of Cellular and Molecular Biology, Jiangsu Province Institute of Chinese Medicine,
Nanjing 210000, P. R. China

[†]Jin-Long Chen and Li Li contributed equally to this work

^{*}Corresponding Author, chenjl_4@hotmail.com; guning@seu.edu.cn

- Fig. S1** (A) UV-vis spectra of reaction mixture as time-course from 0 to 60 min. (B) UV-vis monitoring of the conversion of KMnO_4 ($\lambda_{\text{abs}} = 526 \text{ nm}$) to MnO_2 NSs ($\lambda_{\text{abs}} = 374 \text{ nm}$) from 0 to 60 min (C) Time-course photographs of the reaction mixture from 0 to 60 min
- Fig. S2** Schematic illustration for the lauric acid and SDS co-modified MnO_2 nanosheets formation by in situ redox reaction between KMnO_4 and dodecanol on the surface performed soft-template
- Fig. S3** (A) Photographs of dispersion of MnO_2 NSs in conventional solvents (B) Stability of aqueous solutions of MnO_2 NSs in various pH medium. (C) UV-visible spectra for water-dispersions of various concentrations of MnO_2 NSs (D) The absorbance at 374 nm is plotted against the various concentrations of MnO_2 NSs.
- Fig. S4** The overall fold of GOD obtained from the Protein Data Bank (PDB ID: 1GAL). The theoretical height of compact (B) and stretched (C) structure of single-layer MnO_2 NSs co-modified with lauric acid and SDS, (D) The structures of lauric acid and SDS simulated with ChemBioOffice 2010 (Cambridge Soft Corporation). The theoretical height of single-layer of MnO_2 NSs is about 0.52 nm.
- Fig. S5** pH dependent redoxable reactivity of the as-obtained MnO_2 NSs to ascorbic acid (A), L-glutathione (B), citric acid (C) and H_2O_2 (D), respectively.
- Fig. S6** (A) pH-dependent H_2O_2 -decomposition of MnO_2 NSs. (B) Effect of temperature (B) and time (C) on the decreased absorbance of the presented glucometer composition of $1.5 \mu\text{g mL}^{-1}$ GOD and $35 \mu\text{M}$ MnO_2 NSs in the presence of $20 \mu\text{M}$ glucose.

7. **Fig. S7** (A) Normalized fluorescence excitation (black curve) and emission (red curve) spectra of GOD and UV-vis absorption spectrum of MnO₂ nanosheets (blue curve); Fluorescence spectra of GOD (10 μg mL⁻¹) with the addition of various concentrations of MnO₂ nanosheets. $\lambda_{\text{ex}} = 290$ nm. The concentration of MnO₂ nanosheets was increased from upper to bottom (Insets: Plots of F₀/F against MnO₂ NSs concentration. By contrast of emission profile of GOD before and after addition of MnO₂ NSs).
8. **Table S1**. Comparison of the performances of designated biosensors integrated GOD with conventional nanomaterials for glucose sensing
9. **Fig. S8** FT-IR spectra of MnO₂ NSs, GOD and the glucometer composing of GOD and MnO₂ NSs, respectively
10. **Table S2** Enzymatic conformation of free GOD and GOD noncovalent immobilization on MnO₂ NSs by use of CDpro software
11. **Fig. S9** (A) Absorption Spectra of mice blood serum samples dilution by different folds (B) Spectra of MnO₂ NSs in the GOD, serum samples by 1200 dilution folds and GOD-MnO₂ NSs in the presence of diluted serum samples.

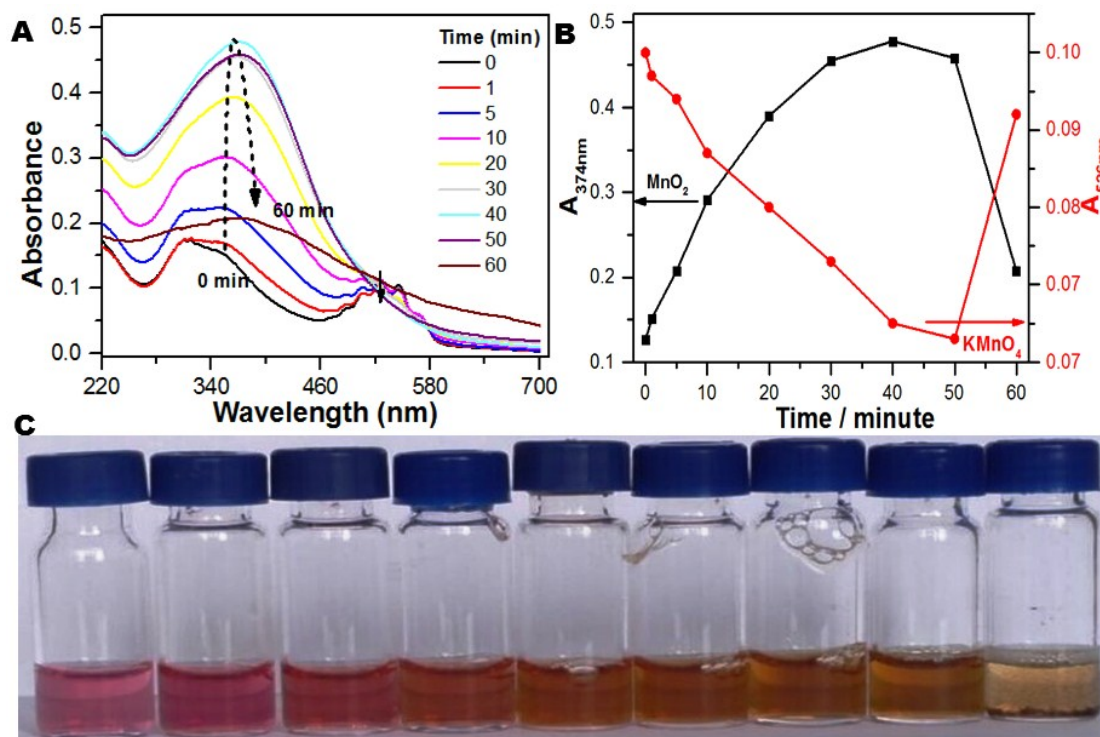


Fig. S1 (A) UV-vis spectra of reaction mixture as time-course from 0 to 60 min. (B) UV-vis monitoring of the conversion of KMnO_4 ($\lambda_{\text{abs}} = 526 \text{ nm}$) to MnO_2 NSs ($\lambda_{\text{abs}} = 374 \text{ nm}$) from 0 to 60 min (C) Time-course photographs of the reaction mixture from 0 to 60 min

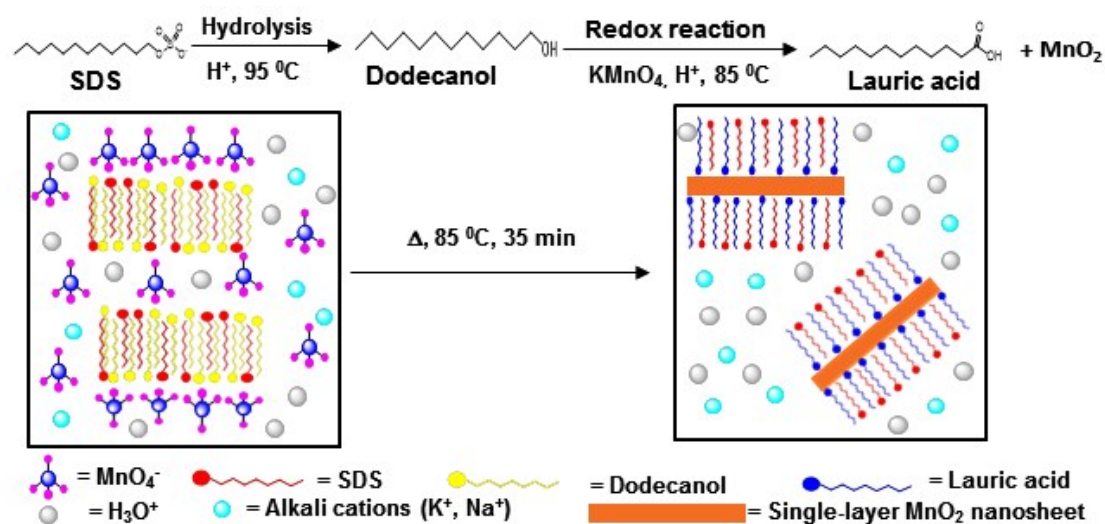


Fig. S2 Schematic illustration for the lauric acid and SDS co-modified MnO_2 nanosheets formation by in situ redox reaction between KMnO_4 and dodecanol on the surface performed soft-template

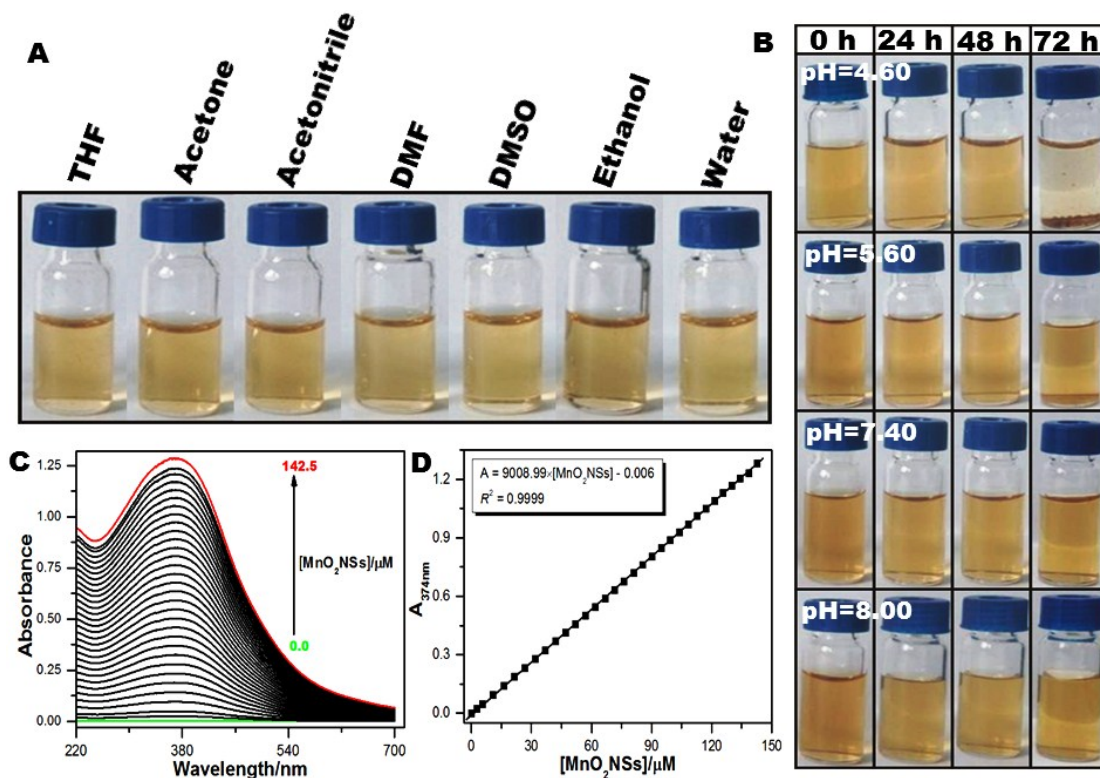


Fig. S3 (A) Photographs of dispersion of MnO₂ NSs in conventional solvents (B) Stability of aqueous solutions of MnO₂ NSs in various pH medium. (C) UV-visible spectra for water-dispersions of various concentrations of MnO₂ NSs (D) The absorbance at 374 nm is plotted against the various concentrations of MnO₂ NSs.

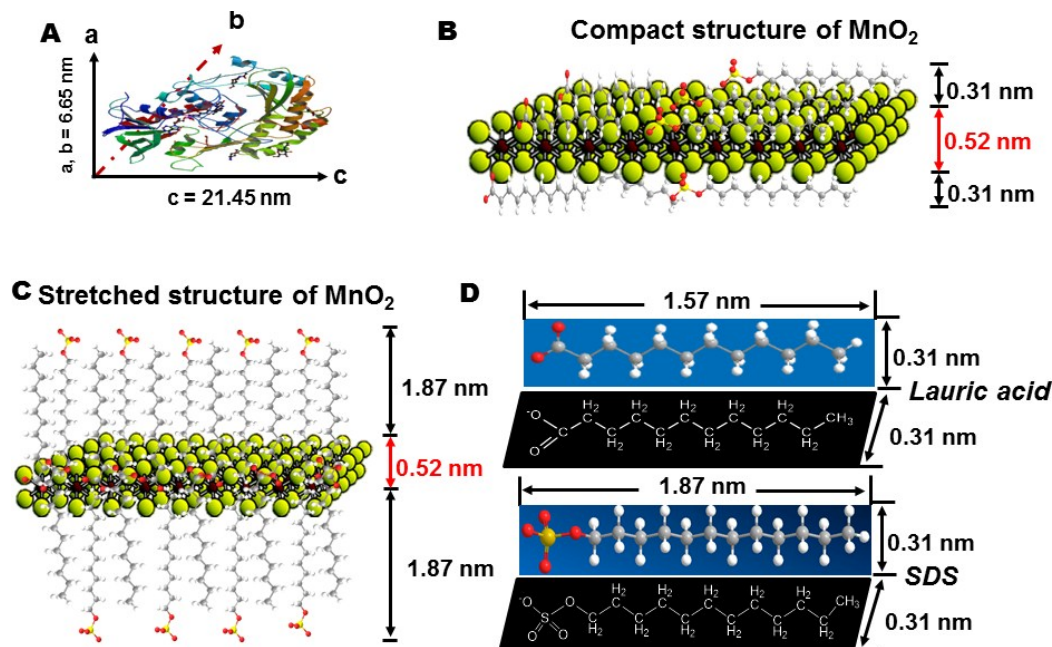


Fig. S4 The overall fold of GOD obtained from the Protein Data Bank (PDB ID: 1GAL). The theoretical height of compact (B) and stretched (C) structure of single-layer MnO₂ NSs co-modified with lauric acid and SDS, (D) The structures of lauric acid and SDS simulated with ChemBioOffice 2010 (Cambridge Soft Corporation). The theoretical height of single-layer of MnO₂ NSs is about 0.52 nm.

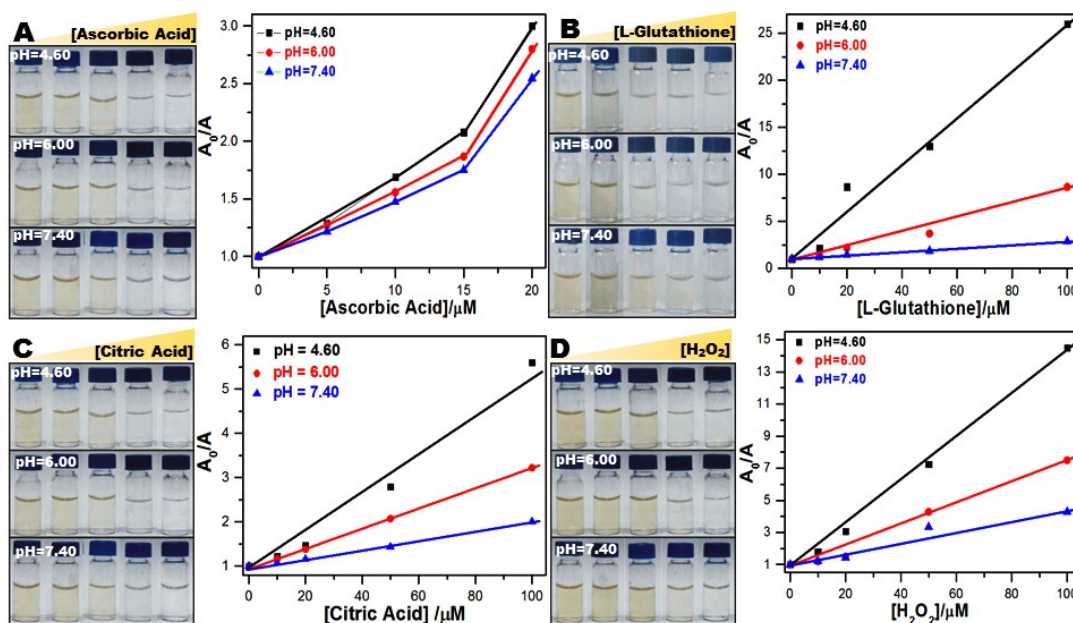


Fig. S5 pH dependent redoxable reactivity of the as-obtained MnO₂ NSs to ascorbic acid (A), L-glutathione (B), citric acid (C) and H₂O₂ (D), respectively.

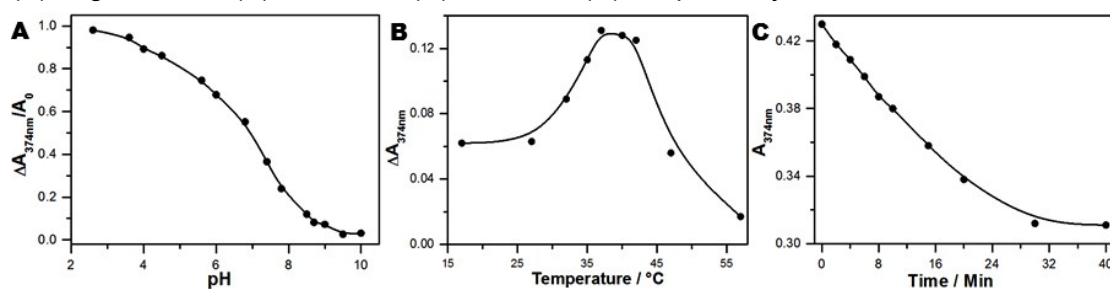


Fig. S6 (A) pH-dependent H₂O₂-decomposition of MnO₂ NSs. (B) Effect of temperature (B) and time (C) on the decreased absorbance of the presented glucometer composition of 1.5 $\mu\text{g mL}^{-1}$ GOD and 35 μM MnO₂ NSs in the presence of 20 μM glucose.

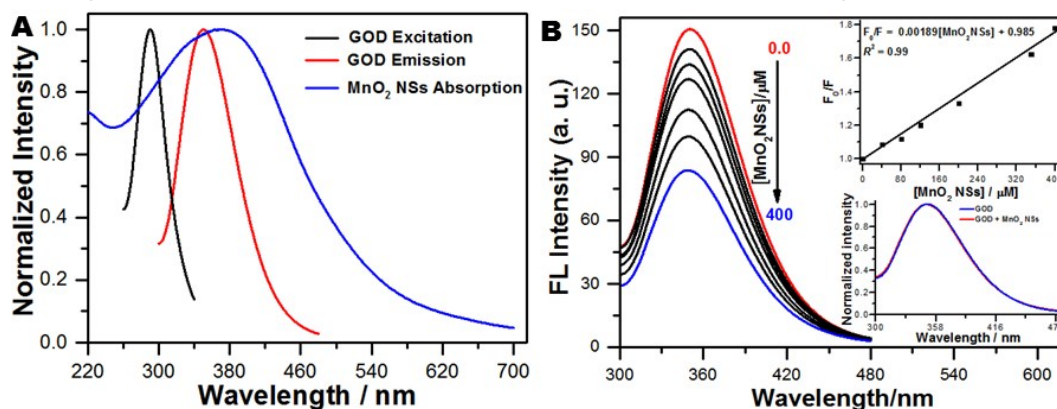


Fig. S7 (A) Normalized fluorescence excitation (black curve) and emission (red curve) spectra of GOD and UV-vis absorption spectrum of MnO₂ nanosheets (blue curve); Fluorescence spectra of GOD (10 $\mu\text{g mL}^{-1}$) with the addition of various concentrations of MnO₂ nanosheets. $\lambda_{\text{ex}} = 290 \text{ nm}$. The concentration of MnO₂ nanosheets was increased from upper to bottom (Insets: Plots of F_0/F against MnO₂ NSs concentration. By contrast of emission profile of GOD before and after addition of MnO₂ NSs).

Table S1. Comparison of the performances of designated biosensors integrated GOD with conventional nanomaterials for glucose sensing

| Nanomaterials | enzyme immobilization | K_m (mM) | Detection mode | LOD (μ M) | Real samples | refs |
|------------------------------------|-----------------------|------------|-------------------------|----------------|--------------|-----------|
| Gold NPs | covalent | 3.74 | spectrophotometry | - | NO | 1 |
| Fe ₃ O ₄ NPs | covalent | 6.8 | fluorescence | - | NO | 2 |
| CdTe QDs | covalent | 0.45 | fluorescence | 0.1 | NO | 3 |
| PMMA microbeads | covalent | 13.79 | spectrophotometry | - | NO | 4 |
| Mn-doped ZnS QDs | covalent | 0.7 | phosphorescence | 3 | Human serum | 5 |
| ZrO ₂ /chitosan | noncovalent | 3.14 | amperometr | 10 | Real blood | 6 |
| ZnO nanorods | noncovalent | 2.90 | amperometr | 10 | NO | 7 |
| CNT | covalent | - | amperometr | 80 | NO | 8 |
| MnO ₂ NPs | Coimmobilization | - | field-effect transistor | 20 | NO | 9 |
| MnO ₂ nanosheets | noncovalent | 0.051 | spectrophotometry | 0.1 | Rat serum | This work |

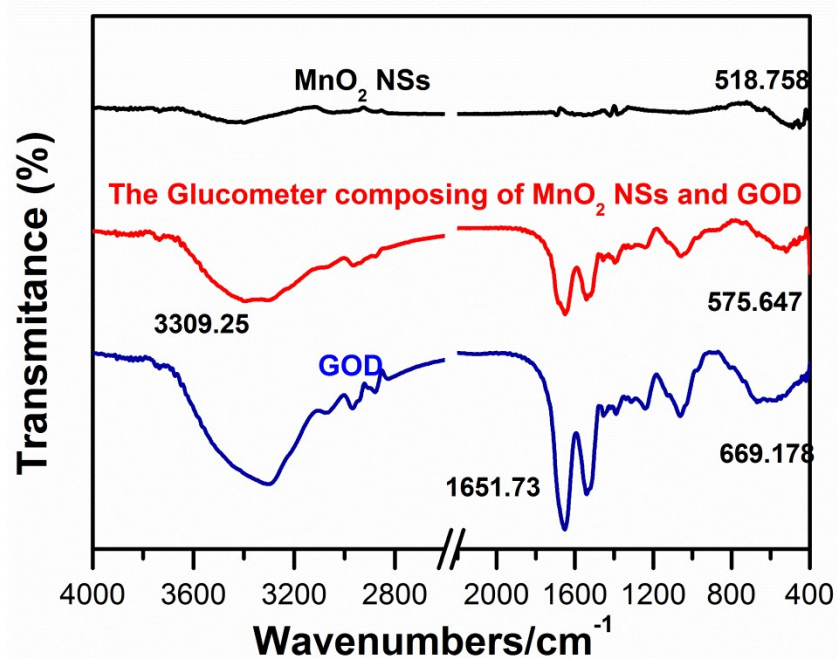


Fig. S8 FT-IR spectra of MnO₂ NSs, GOD and the glucometer composing of GOD and MnO₂ NSs, respectively.

Table S2 Enzymatic conformation of free GOD and GOD noncovalent immobilization on MnO₂ NSs by use of CDpro software

| Enzymatic conformation | Free GOD | | Immobilized GOD | |
|------------------------|----------|-----------------------|-----------------|-----------------------|
| | Fraction | Percentage of content | Fraction | Percentage of content |
| α -helix | 1.230 | 25.7% | 0.985 | 17.3% |
| β -sheet | 1.231 | 25.7% | 1.741 | 30.6% |
| β -turn | 0.950 | 19.8% | 1.221 | 21.4% |
| Radom coil | 1.380 | 28.8% | 1.758 | 30.7% |
| Total | 4.791 | 100% | 5.705 | 100% |
| α/β | 1.0 | | 0.672 | |

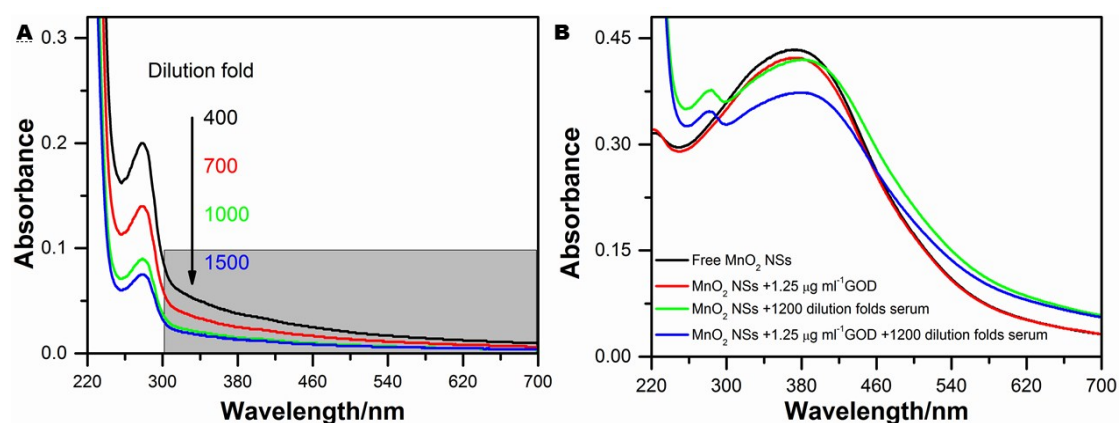


Fig. S9 (A) Absorption Spectra of mice blood serum samples dilution by different folds (B) Spectra of MnO₂ NSs in the GOD, serum samples by 1200 dilution folds and GOD-MnO₂ NSs in the presence of diluted serum samples.

Reference

- Pandey, P.; Singh, S. P.; Arya, S. K.; Gupta, V.; Datta, M.; Singh, S.; Malhotra, B. D., Application of Thiolated Gold Nanoparticles for the Enhancement of Glucose Oxidase Activity. *Langmuir* **2007**, *23* (6), 3333-3337.
- Rossi, L. M.; Quach, A. D.; Rosenzweig, Z., Glucose oxidase-magnetite nanoparticle bioconjugate for glucose sensing. *Anal. Bioanal. Chem.* **2004**, *380* (4), 606-613.
- Cao, L.; Ye, J.; Tong, L.; Tang, B., A New Route to the Considerable Enhancement of Glucose Oxidase (GOx) Activity: The Simple Assembly of a Complex from CdTe Quantum Dots and GOx, and Its Glucose Sensing. *Chemistry – A European Journal* **2008**, *14* (31), 9633-9640.
- Bulmuş, V.; Ayhan, H.; Pişkin, E., Modified PMMA monosize microbeads for glucose oxidase immobilization. *Chemical Engineering Journal* **1997**, *65* (1), 71-76.
- Wu, P.; He, Y.; Wang, H.-F.; Yan, X.-P., Conjugation of Glucose Oxidase onto Mn-Doped ZnS Quantum Dots for Phosphorescent Sensing of Glucose in Biological Fluids. *Anal. Chem.* **2010**, *82* (4), 1427-1433.
- Yang, Y.; Yang, H.; Yang, M.; liu, Y.; Shen, G.; Yu, R., Amperometric glucose biosensor based on a surface treated nanoporous ZrO₂/Chitosan composite film as immobilization matrix. *Analytica Chimica Acta* **2004**, *525* (2), 213-220.
- Wei, A.; Sun, X. W.; Wang, J. X.; Lei, Y.; Cai, X. P.; Li, C. M.; Dong, Z. L.; Huang, W., Enzymatic glucose biosensor based on ZnO nanorod array grown by hydrothermal decomposition. *Applied Physics Letters* **2006**, *89* (12), 123902.
- Lin, Y.; Lu, F.; Tu, Y.; Ren, Z., Glucose Biosensors Based on Carbon Nanotube Nanoelectrode Ensembles. *Nano Letters* **2004**, *4* (2), 191-195.
- Luo, X.-L.; Xu, J.-J.; Zhao, W.; Chen, H.-Y., A novel glucose ENFET based on the special reactivity of MnO₂ nanoparticles. *Biosensors and Bioelectronics* **2004**, *19* (10), 1295-1300.